PHYSICAL REVIEW B VOLUME 32, NUMBER 12 15 DECEMBER 1985

Interface chemistry of ternary semiconductors: Local morphology of the $Hg_{1-x}Cd_xTe(110)$-Cr interface

A. Franciosi and P. Philip
Department of Chemical Engineering and Materials Science, University of Minnesota, Minneapolis, Minnesota 55455

D. J. Peterman
McDonnell Douglas Research Laboratories, St. Louis, Missouri 63166

(Received 18 April 1985)

Synchrotron-radiation photoemission studies of interfaces prepared *in situ* on cleaved substrates show atomic interdiffusion with Cr/Hg and Cr/Cd exchange reactions taking place at room temperature for Cr coverages less than 2 Å. Correspondingly, dissociated Te is released at the surface. A subsurface region 10—13 Å thick is formed in which Cr atoms replace all of the Hg atoms and at least 20% of the Cd atoms. Below this subsurface the semiconductor maintains the bulk stoichiometry and the initial surface band bending.

Very little is known about the interface chemistry of ternary semiconductor alloys. The results available on compound semiconductors[1,2] can be extrapolated only in part to ternary alloys, where the interplay of two different kinds of chemical bonding can substantially change the character and stability of each bond with respect to those of the binary parent compounds. $Hg_{1-x}Cd_xTe$ is probably the ternary semiconductor most studied in recent years because of its widespread application for infrared detectors in the (8—14)-μm spectral range. This material poses a number of intriguing fundamental and technological problems that only now are starting to be addressed. As a ternary semiconductor alloy formed from parent compounds of very different stability, this material easily sustains composition variations. It has also been recently recognized that the interplay of ionicity and metallicity in the two kinds of chemical bonding that coexist in the matrix further weakens[3,4] one bond (Hg—Te) relative to the other (Cd—Te), causing lattice, surface, and interface instabilities in the alloy.[5] For example, dramatic composition variations have been observed in $Hg_{1-x}Cd_xTe$ as a result of processes as diverse as mechanical damage,[6,7] oxidation,[8] and metal deposition.[9,10] A detailed understanding of the interface chemistry and physics of this material requires a systematic analysis of variations in local stoichiometry, Schottky-barrier height, and interface width.

Pioneering photoemission studies have recently clarified the nature of chemical bonding in the bulk alloy,[11,12] and related the Schottky barrier height for the $Hg_{1-x}Cd_xTe(110)$-Al (Ref. 10) and $Hg_{1-x}Cd_xTe(110)$-Au (Ref. 13) interfaces to the local composition of the semiconductor surface layer. In this paper we focus on the chemistry of $Hg_{1-x}Cd_xTe$-refractory metal interfaces, which represent a new class of technologically important junctions that are largely unexplored. We have performed synchrotron radiation photoemission studies of the $Hg_{1-x}Cd_xTe(110)$-Cr interface formed *in situ*. Results concerning the connection between Schottky-barrier height and the changes in semiconductor surface composition have been presented earlier.[14] Here we describe the local morphology of the interface region in detail and relate the interface electronic properties to the local chemistry of the material.

EXPERIMENTAL DETAILS

Single crystals of $Hg_{1-x}Cd_xTe$ were prepared at McDonnell Douglas using a modified Bridgman method. Several oriented (110) posts ($3\times3\times15$ mm^3) were cut from the center of the cylindrical portion of a boule. Samples cut from each end of the cylinder showed an identical energy gap of 0.175 ± 0.01 eV and p-type conductivity with a room-temperature carrier concentration of 2×10^{16} cm^{-3}, as determined from infrared-transmission and Hall-effect measurements, respectively. The sample composition, deduced from the band gap measurements[15] was $x=0.22\pm0.01$. The posts were loaded into the photoelectron spectometer through a special fast-insertion device, thus allowing an operating pressure $<5\times10^{-11}$ Torr while avoiding sample exposure to high temperature. The posts were cleaved *in situ* with varying degrees of success at obtaining mirrorlike surfaces. The photoemission measurements were performed by positioning the samples at the common focus of the monochromatic photon beam and a commercial double pass cylindrical mirror analyzer. Photoelectron energy distribution curves (EDC's) were recorded for $40\leq h\nu\leq140$ eV using a "grasshopper" grazing incidence monochromator and synchrotron radiation from the 240-MeV electron storage ring, Tantalus, at the Synchrotron Radiation Center of the University of Wisconsin—Madison. The overall energy resolution (electrons plus photons) ranged from 0.4—0.7 eV for $h\nu<100$ eV to about 0.8—1.0 eV for the high-photon-energy studies (Te 4d and Cr 3p core levels at $h\nu=110$ eV). The interfaces were prepared *in situ* by direct Cr sublimation from a W coil and the metal coverage was monitored using a quartz thickness monitor.

RESULTS

Valence states

The experimental results are organized in two series of figures. Figures 1—4 show valence-band spectra for the clean and Cr-covered $Hg_{1-x}Cd_xTe$ surfaces, Figs. 5—10 summarize results for the core-level emission. In the photon-energy range available to us we were able to monitor the evolution of the Hg $5d$, Cd $4d$, Te $4d$, and Cr $3p$ core levels as a function of metal coverage, gaining information on the relative concentration and on the local chemical environment of each atomic species present in the interface region.

In Fig. 1 we show representative energy distribution curves for the valence-band emission of the cleaved $Hg_{1-x}Cd_xTe$ surface. The zero of the binding energy scale corresponds to the spectrometer Fermi level as derived from the Fermi level cutoff of the high-Cr-coverage EDC's. The spectra have been approximately normalized to the main emission features, and are given in arbitrary units. The EDC's show good qualitative agreement with the results of Silberman *et al.*[11] and exhibit a Tep—derived density-of-states feature within 3.5 eV of the Fermi level E_F, and a second structure between 4 and 7 eV derived primarily from unresolved Cd s and Hg s features which reflect the metal s—chalcogenide p hybridization responsible for the stability of the alloy.[16]

The emission features between 8 and 12 eV correspond to the Hg $5d$ and Cd $4d$ core levels. Deconvolution of two doublets was performed using the experimental line shape of the Hg $5d$ and Cd $4d$ levels obtained from cleaved HgSe and CdSe samples. As an example, the result of the decomposition for the clean surface is shown in the top section of Fig. 6. All cleaves resulted in identical [Hg]:[Cd]:[Te] ratios (as determined by the ratios of the Hg $5d$, Cd $4d$, and Te $4d$ integrated emissions) irrespective of cleave quality, and no time-dependent change of the surface composition was observed after cleaving. From the EDC's of Fig. 1 it is possible to estimate the position of the valence band maximum, E_v, by linearly extrapolating the valence band edge at low binding energy. From all cleaves we obtained $E_v=0.49\pm0.15$ which, when compared with the measured bulk band gap of only 0.175 ± 0.01 eV, indicates a strongly inverted (n-type) character for the near surface region.

The effect of Cr deposition on the valence band emission is shown in Fig. 2 for $h\nu=60$ eV. The bottom-most spectrum is the clean surface spectrum while EDC's displaced upward correspond to increasing Cr coverages Θ and are given in relative units. Two effects are clearly evident in Fig. 2. First, emission from the Cr $3d$ states quickly dominates the valence band spectra within 3 eV of E_F. Second, the Hg-derived emission decreases dramatically and is almost negligible at $\Theta\sim3$ Å. These two trends are shown in more detail in Figs. 3 and 5 where we have plotted, in an expanded scale, the valence-band emission within 9 eV of E_F and the Hg $5d$—Cd $4d$ core emission, respectively. In Fig. 3 we see that initial Cr deposition gives rise to increased valence emission within 2 eV of E_F, and to a "tailing" of valence states at E_F. A true Fermi-level cutoff, however, cannot be seen until $\Theta\sim3$ Å.

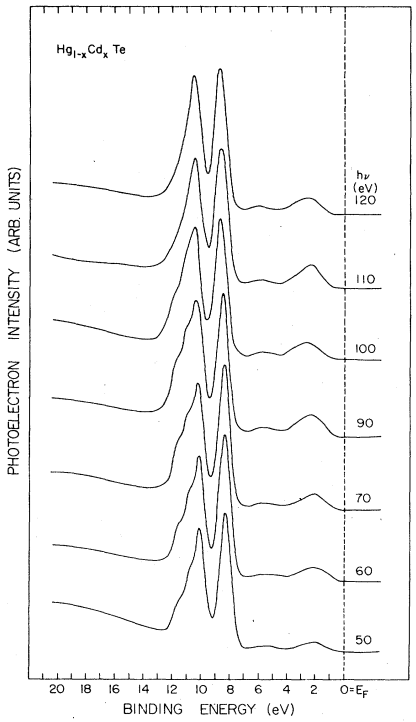

FIG. 1. EDC's for the valence-band and Hg $5d$—Cd $4d$ core-level emissions from $Hg_{1-x}Cd_xTe(110)$ surfaces obtained by cleaving $x=0.22$ bulk crystals.

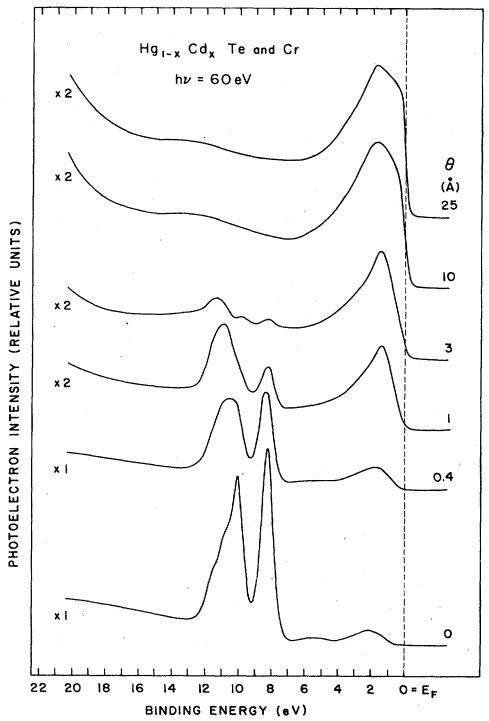

FIG. 2. Valence-band and Hg $5d$—Cd $4d$ core-level emissions for the $Hg_{1-x}Cd_xTe(110)$-Cr interface. The topmost spectra are shown multiplied by a scale factor of 2.

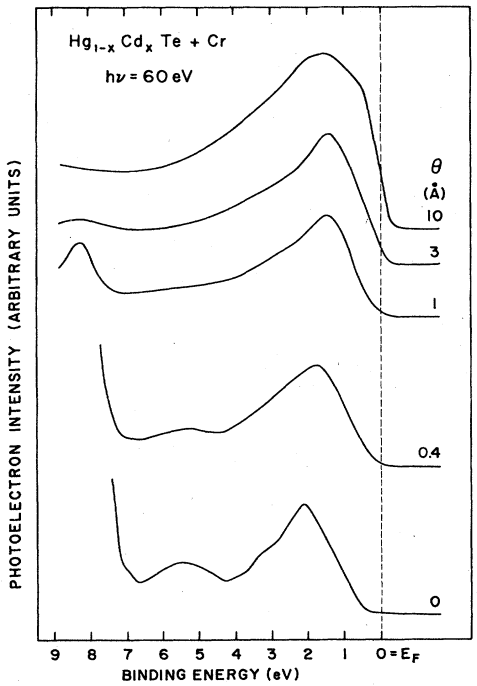

FIG. 3. Detail of the valence-band emission within 9 eV of the Fermi level E_F for the $Hg_{1-x}Cd_xTe(110)$-Cr interface. Initial Cr deposition gives rise to increased valence emission within 2 eV of the E_F and to tailing of valence states at E_F. A true Fermi level cutoff, however, can be seen only for coverages $\Theta \geq 3$.

At this point, the $3d$ emission gives rise to a main emission feature centered 1.3—1.4 eV below E_F which is relatively sharp [full width at half maximum (FWHM) ~2.7—2.8 eV] compared to the more bulklike Cr emission at $\Theta = 25$ Å. Very little change of the valence states is observed for $10 < \Theta < 25$ Å yet there are several relevant differences compared to bulk Cr. This is shown in Fig. 4 where the topmost spectrum (solid line) was obtained from a 250-Å-thick Cr film evaporated on oxidized Ta, and the bottom-most spectrum from the $Hg_{1-x}Cd_xTe$ interface with $\Theta = 25$ Å [coverage corresponding to over 30 monolayers, taking 1 ML $= 6.8 \times 10^{14}$ atoms /cm^2 equals the total surface atomic density for $Hg_{1-x}Cd_xTe(110)$]. The main differences we note (tic marks) are a shift of the main $3d$ feature by 0.2 eV to higher binding energy, increased emission within 1 eV of the Fermi level, and a rather broad density-of-states feature centered 12.5 eV below E_F.

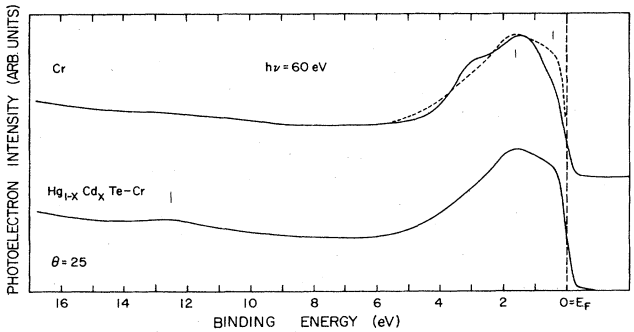

FIG. 4. Comparison of valence emission from bulk Cr (250 Å Cr film on oxidized Ta) and from the $Hg_{1-x}Cd_xTe$-Cr interface at $\Theta = 25$ Å. The 25-Å-coverage interface shows increased emission within 1 eV below E_F and a 0.2-eV shift to higher binding energy of the main $3d$ feature.

Core emission

Figure 5 shows the evolution of the Hg $5d$ and Cd $4d$ core-level line shapes in the $0 \leq \Theta \leq 3$ Å coverage range for $h\nu = 60$ eV. The spectra were obtained from the EDC's of Fig. 2 after subtraction of a smooth secondary electron background and are given in relative units. The vertical dashed lines mark the position of the Hg $5d_{5/2}$, Hg $5d_{3/2}$, and Cd $4d_{5/2}$ levels after deconvolution (see top section of Fig. 6). Emission from all cores appear strongly attenuated even at low metal coverages (note the scale factors in Fig. 5). Furthermore, the Hg-to-Cd ratio decreases dramatically with increasing metal coverage. The binding energy of the Hg $5d$ core levels remains unchanged as a function of metal coverage within experimental uncertainty (~0.1 eV). For the Cd core levels, our data show constant binding energy for $\Theta \leq 1$ Å, and suggest a sharp 0.3—0.4 eV binding energy increase for 1 Å $< \Theta < 3$ Å.[17]

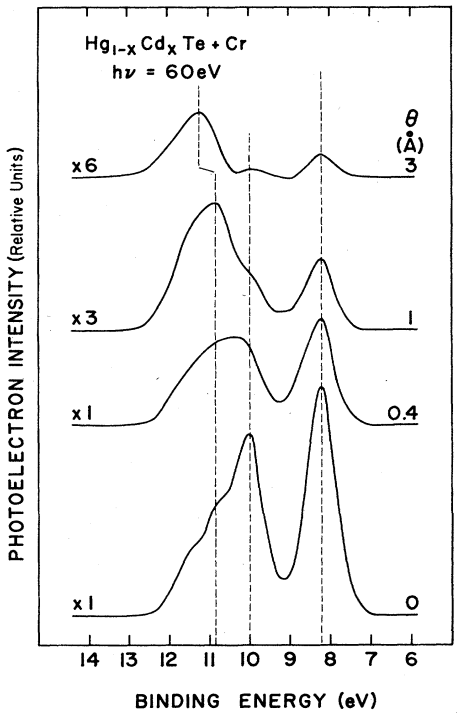

FIG. 5. Detail of the Hg $5d$ and Cd $4d$ core-level emission from the $Hg_{1-x}Cd_xTe$-Cr interface as a function of metal coverage. The vertical dashed lines indicate the corresponding binding energy as derived from the deconvolution shown in the top section of Fig. 6. Note the dramatic increase of the [Cd]/[Hg] ratio due to Hg migration away from the subsurface layer.

To examine quantitatively the surface concentration of Hg and Cd as a function of coverage, the two doublets were deconvolved as sketched in the top sections of Fig. 6. The total integrated intensity of each doublet at a given coverage Θ was normalized to the zero-coverage emission intensity, and is shown in a semilogarithmic plot in the lower section of Fig. 6. The solid lines correspond to an exponential attenuation of the core emission. The resulting attenuation lengths[18] are 0.7 and 1.7 Å, respectively, for the Hg $5d$ and Cd $4d$ core levels. The attenuation of the Cd and especially of the Hg core emission is far more rapid than can be reasonably expected from an escape-depth-driven mechanism, where an attenuation length of 4–5 Å would be expected.[19]

EDC's for the Te $4d$ core emission at $h\nu=110$ eV and $h\nu=53$ eV are shown (solid lines) in Figs. 7 and 8, respectively. The spectra appear all approximately normalized to the main emission feature to emphasize the line shape changes. The EDC's (solid lines) in Fig. 7 show that the sharp experimental $4d$ line shape for the clean surface is broadened asymmetrically at $\Theta=1.5$ and 3.0 Å and shifted to lower binding energy. For $\Theta\geq 10$ Å, however, the linewidth decreases again while the doublet is shifted to higher binding energy. These nonmonotonic trends can be explained by the existence of two $4d$ lines, shifted by 0.5 eV from each other, and with coverage-dependent relative intensity. To fit the experimental spectra, we used two $4d$ line shapes obtained from the clean surface emission and, as fitting parameters, the binding energy and relative intensity of the two $4d$ components. The result of the fit is shown in Fig. 7 by a short-dashed line. The fit is remarkably good, and the experimental line shape appears to be composed of a low binding energy doublet (Te $4d$ I) that dominates at low coverage, and by a new high-binding-

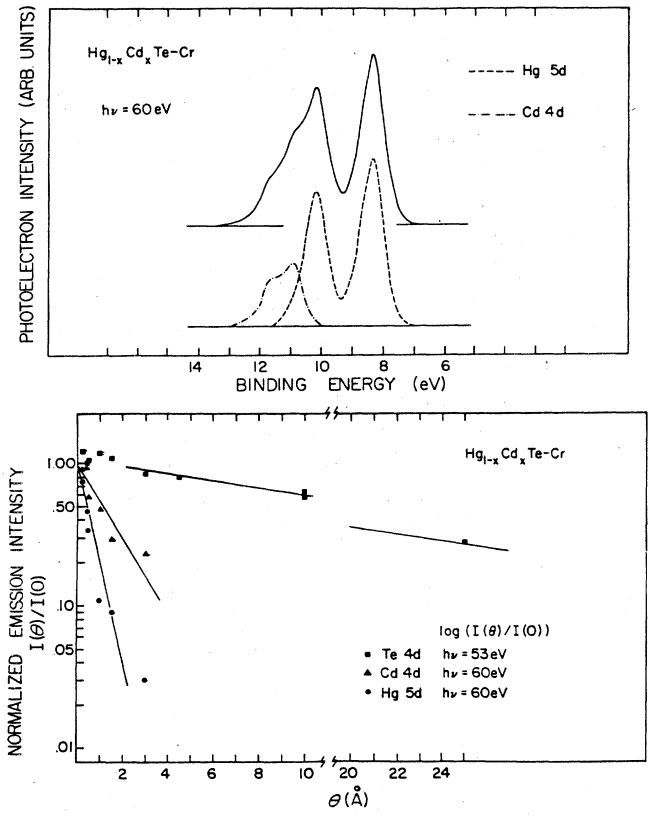

FIG. 6. Top: deconvolution of the experimental line shape (solid line) in Hg $5d$ (dashed line) and Cd $4d$ (dotted-dashed line) contributions for the clean $Hg_{1-x}Cd_xTe$ surface. The $4d$ and $5d$ line shapes were obtained from HgSe and CdSe samples. Bottom: semilogarithmic plot showing the integrated intensity of the Hg $5d$, Cd $4d$, and Te $4d$ core-level emission, normalized to the emission from the clean surface, as a function of metal coverage. As discussed in the text, the fast attenuation of the Hg and Cd emission reflects an exchange reaction in a (10–13)-Å subsurface region, where all of the Hg atoms and at least 20% of the Cd atoms are replaced by Cr atoms.

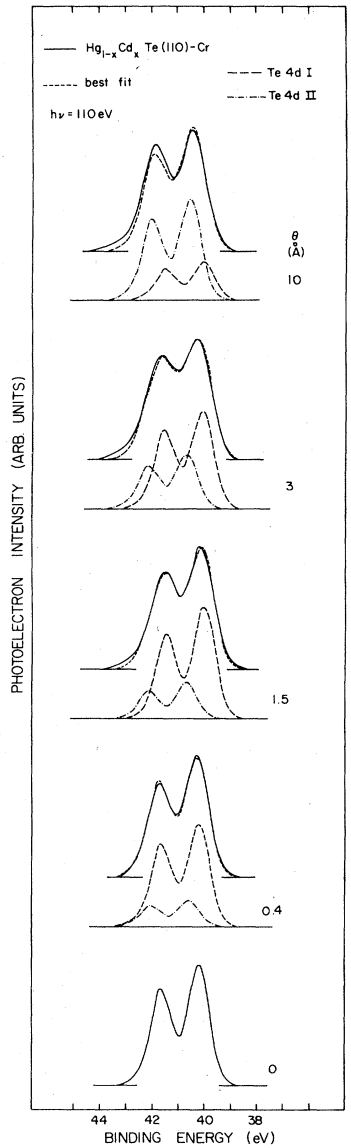

FIG. 7. Te $4d$ core emission from the $Hg_{1-x}Cd_xTe$-Cr interface at $h\nu=110$ eV. Solid line: experiment. Short-dashed line: results of a best fit using the sum of a Te $4d$ I subsurface component (long-dashed line) and a Te $4d$ II surface component (dotted-dashed line). At $h\nu=110$ eV the emission from the Cr $3p$ cores is negligible for $\Theta\leq 10$.

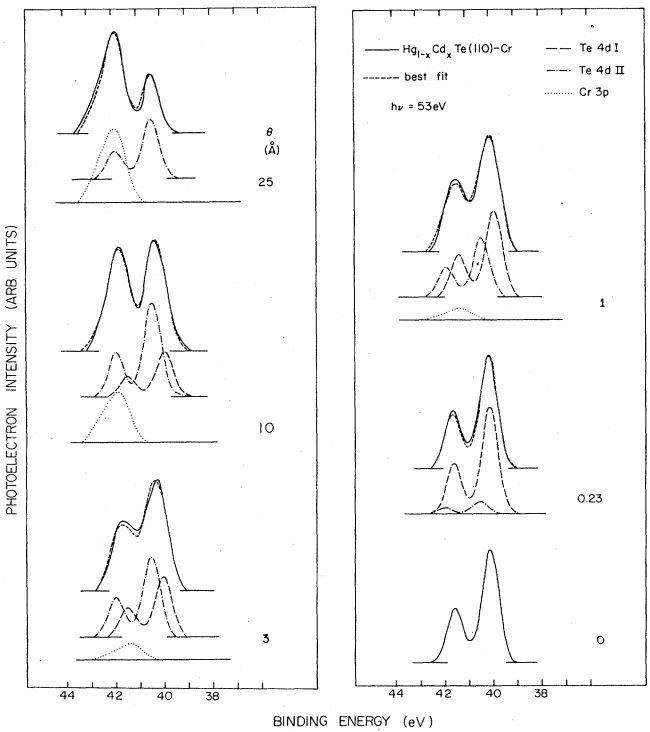

FIG. 8. Te 4*d* core emission from the $Hg_{1-x}Cd_xTe$-Cr interface at $h\nu=53$ eV. Solid line: experiment. Short-dashed line: result of a best fit using the sum of a Te 4*d* I subsurface component (long-dashed line), a Te 4*d* II surface component (dotted-dashed line), and a Cr 3*p* line (dotted line). The Cr line shape was obtained from a Cr film evaporated on an inert substrate. At $h\nu=53$ eV we are near the photoemission threshhold and the Cr signal is of the same order of magnitude as the Te signal.

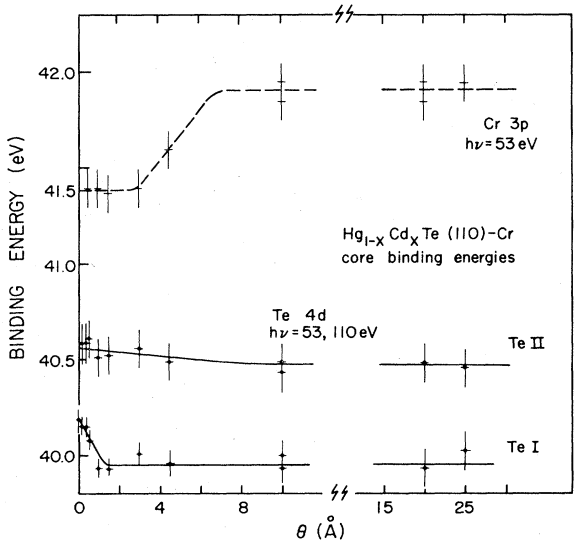

FIG. 9. Binding energy of the Cr 3*p*, Te 4*d* I, and Te 4*d* II, core-level emission from the $Hg_{1-x}Cd_xTe$-Cr interface. The binding energies were obtained from the deconvolution procedure described in Figs. 7 and 8. The high-coverage saturation values of the Cr 3*p* and Te 4*d* II binding energies are close to the elemental values.

energy component (Te 4*d* II) 0.45 eV above the main line that grows as a result of Cr deposition, and becomes the dominant feature at $\Theta=10$ Å. At coverages greater than 10 Å the Cr 3*p* core-level contribution, at a binding energy of about 42 eV, is not negligible, even for $h\nu=110$ eV, and the fit cannot be obtained by simply superimposing two Te 4*d* lines. This is demonstrated by the results at $h\nu=53$ eV in Fig. 8. At photon energies close to the photoemission threshold, one expects the centrifugal barrier to emphasize the Cr 3*p* as compared to the Te 4*d* emissions in our EDC's. The experimental line shapes in Fig. 8 (solid line) reflect, in fact, the superposition of the two 4*d* lines and a Cr 3*p* line (dotted line). Again, to reduce the number of fitting parameters, we used an experimental Cr 3*p* line shape determined from evaporated Cr films, and we let the binding energy and intensity of this line be the additional fitting parameters. The results (shown with short-dashed lines in Fig. 8) were extremely rewarding. We emphasize that the results of the fitting at $h\nu=53$ eV confirm those at $h\nu=110$ eV since the binding energy of each Te 4*d* line was identical, within experimental uncertainty, in the two cases. The binding energy of each Te component and of the Cr 3*p* line is shown in Fig. 9. The Cr 3*p* emission appears initially at constant binding energy (for $\Theta\leq 3$ Å) and then shifts toward higher binding energy. The final binding energy at high metal coverage appears close to the bulk Cr value (41.95 ± 0.1 eV versus 42.22 ± 0.15 eV). The binding energy of the Te 4*d* II component remains relatively unchanged as a function of coverage, with at most a gradual 0.1-eV decrease in the whole coverage range. The Te 4*d* I component, that starts at the clean surface position, shifts rigidly 0.25 eV to lower binding energy during initial metal deposition ($\Theta\leq 2$ Å) and then remains unchanged. The integrated intensity of each Te 4*d* component is plotted in Fig. 10 as a function of metal coverage for $h\nu=53$ eV. The overall Te 4*d* core-level emission (component I plus component II) is compared in the lower part of Fig. 6 (full squares) with the Cd 4*d* and Hg 5*d* core-level emission. It is readily seen from Fig. 6 that the attenuation of the Te 4*d* core-level emission is relatively small compared to that of the Cd and Hg core-level emissions. This is because while the Te 4*d* I component exponentially decreases in intensity (lower section, Fig. 10) the Te 4*d* II component (upper section, Fig. 10) grows dramatically during deposition of the first two monolayers. The results at $h\nu=110$ eV are similar, except for the higher saturation value of the Te 4*d* II emission, about 60—80% of the clean surface emission as opposed to 40%.

DISCUSSION

Composition variations

The results of Figs. 1—10, and in particular, of Figs. 2, 3, 9, and 10, suggest that different processes occur at the interface in the low-coverage range $0\leq\Theta<2$ Å, and in the high-coverage range $\Theta>2$ Å. In Fig. 6 we showed that dramatic changes in the relative [Hg]/[Te] and [Hg]/[Cd] concentrations at the surface occur upon Cr deposition at low coverage. For 2 Å Cr coverage the

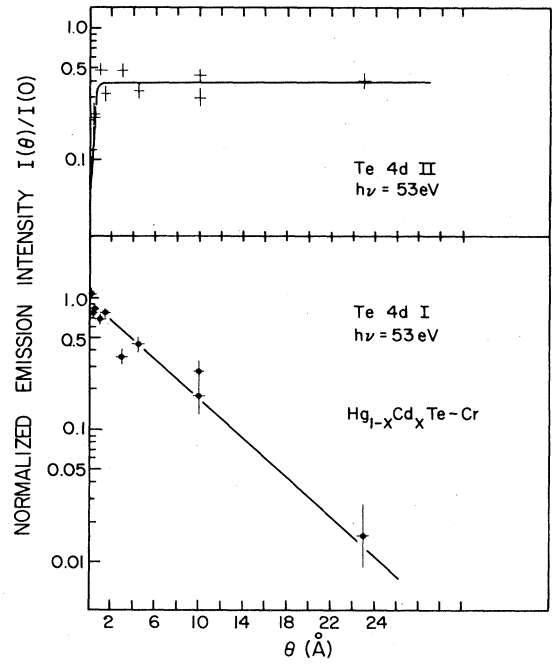

FIG. 10. Semilogarithmic plot of the integrated emission intensity of the Te 4*d* core levels from the $Hg_{1-x}Cd_xTe$-Cr interface, normalized to the Te 4*d* emission from the clean surface. Top: The Te 4*d* II component corresponds to dissociated Te released at the surface during the first interface formation stage. Bottom: The Te 4*d* I component corresponds to Te atoms in the subsurface layer, where the Cr-Hg (and Cr-Cd) exchange reaction takes place for $\Theta \leq 2$ Å.

Hg 5*d* core-level emission is reduced to about 4% of the initial value, the Cd 4*d* emission to about 30%, while the overall Te 4*d* emission remains near the clean surface value (100 %). The reduction of the Hg signal is explained by a combination of three experimental observations: (a) Hg depletion of the semiconductor surface layer, (b) layer-by-layer Cr coverage of the reacted surface, and (c) Te outdiffusion at the surface of the Cr film. The analysis of the Te 4*d* line shape gives us a guideline to interpret the remaining experimental results. Figures 7 and 8 show that two well-defined chemical environments exist for the Te atoms at the surface. The Te 4*d* I environment is related to the bulk semiconductor $Hg_{0.78}Cd_{0.22}Te$ environment, as indicated by the Te 4*d* I binding energy which starts at the clean surface value (and then shifts rigidly to lower binding energy; see Fig. 9). The Te 4*d* II environment is sharply different from the initial semiconductor environment, as indicated by the (0.4—0.5)-eV increase in 4*d* binding energy, which varies very little with further metal deposition (Fig. 9). The intensities of the Te 4*d* I and Te 4*d* II components (Fig. 10) exhibit sharply different coverage dependencies. The Te 4*d* II component increases dramatically at low coverage ($\Theta < 2$ Å), with a suggestive inverse relationship to the sharp decrease of the Hg 5*d* emission (Fig. 6). At higher coverage it saturates to a constant limit of about 40% of the initial overall Te emission ($h\nu = 53$ eV). The saturation value at $h\nu = 110$ eV is, instead, about 70%. Because of the shorter escape depth at $h\nu = 110$ eV, this last point clearly indicates the surface character of the Te 4*d* II emission. It is possible to roughly estimate the amount of Te at the film surface by calculating the thickness d of a Te layer which would give rise to the same 4*d* emission intensity observed at the highest metal coverage. Assuming the Te photoionization cross section to be similar in the semiconductor and in the Te 4*d* II environment, one obtains

$$\left.\frac{I^{\mathrm{II}}_{\mathrm{Te}}(\Theta)}{I_{\mathrm{Te}}(0\ \text{Å})}\right|_{\Theta\to\infty} \simeq 1 - e^{-d/L},$$

where L is the photoelectron escape depth [$L \simeq 4$ Å at $h\nu = 110$ eV and $L \simeq 8$ Å at $h\nu = 53$ eV (Ref. 19)]. For both $h\nu = 53$ eV and $h\nu = 110$ eV we obtain $d \simeq 3$ Å, i.e., about 1.3 monolayers, in terms of the Te surface atomic density on the $Hg_{0.78}Cd_{0.22}Te(110)$ surface. The Te 4*d* II emission is therefore localized in a relatively thin surface layer of the deposited film. Further information on the chemical environment of the Te 4*d* II component can be obtained from the high-coverage Cr 3*p* (Fig. 9) and valence-band (Fig. 4) results. At high metal coverages ($\Theta \sim 25$ Å) the Te 4*d* I emission does not contribute appreciably (Fig. 10) and the results of Figs. 4 and 9 reflect the interaction of the Te 4*d* II species with the top layers of the Cr film. Correspondingly, the Te 4*d* II binding energy (0.4—0.5 eV above the initial 4*d* substrate emission) is consistent with the "elemental Te" core binding energies reported in Refs. 20 and 21, and the Cr 3*p* binding energy is close to the elemental Cr 3*p* value. This suggests a relatively small Cr-Te interaction for the Te 4*d* II environment. The valence band results of Fig. 4 are qualitatively consistent with such a picture. An elemental Te valence emission is expected to show[22] a 5*s* emission feature peaked some 12 eV below the valence band edge and a leading emission feature within 1.5 eV of the valence band edge, deriving from the Te lone-pair *p* electrons. Figure 4 shows that the high-coverage valence-band spectra exhibit indeed a 12.5-eV broad emission feature absent in Cr and increased emission within 1 eV from E_F. We therefore suggest that the Te 4*d* II species that are released at the surface during the early stages of interface formation reflect mostly an elemental Te environment.

The sharp decrease of the Hg 5*d* emission (Fig. 6) for $\Theta < 2$ Å cannot be explained simply by layer-by-layer coverage of the $Hg_{1-x}Cd_xTe$ substrate, even if one takes into account the formation of an additional Te 4*d* II surface layer. Hg has to migrate away from the surface layer. Since the binding energy of the Hg 5*d* cores (Fig. 5) remains unchanged, this process is likely to produce a surface layer completely depleted of Hg rather than a layer with graded Hg content. In the first case one would expect the residual Hg emission to come from deeper in the solid and to reflect a relatively unperturbed $Hg_{1-x}Cd_xTe$ environment. In the second case one would expect, instead, several inequivalent environments for Hg atoms within the experimental sampling depth, with consequent broadening and shift of the Hg 5*d* cores, in contrast with the results of Fig. 5. The residual 4% Hg 5*d* emission observed in Fig. 5 at $\Theta = 2$ Å, is consistent with complete Hg depletion of a (13—16)-Å thick surface layer.[23]

The residual Hg core emission would then reflect the stoichiometric $Hg_{1-x}Cd_xTe$ semiconductor below this layer. The Te emission, instead reflects both the dissociated species at the surface of the evaporated film (Te 4*d* II) and the reacted Te 4*d* I species in the subsurface layer (see next section). We emphasize that at $\Theta=2$ Å only an estimated 10—15% of the Te 4*d* I emission ($h\nu=53$ eV) originates from regions of the semiconductor deep enough in the solid so to reflect the stoichiometric situation.

Exchange reactions

In the lower part of Fig. 10 we show that the intensity of the Te 4*d* I core-level emission ($h\nu=53$ eV) decreases to about 70% of its initial value for $\Theta\sim2$ Å and, at higher metal coverages, follows an exponential behavior with attenuation length of 7—8 Å. Since this value is consistent, within experimental uncertainty, with the photoelectron escape depth, we identify the Te 4*d* I component as Te subsurface emission. Our results show, therefore, no evidence of Cr-Te interdiffusion at high metal coverages ($\Theta>2$ Å). For $\Theta\leq2$ Å, the interpretation of the results of Fig. 10 is complicated by the outdiffusion of Te 4*d* II species and by Hg migration away from the surface. For $\Theta\sim2$ Å we note that the observed Te 4*d* I intensity (70%) is consistent with the attenuation expected from the Te 4*d* II layer alone, as if the Cr did not contribute to the attenuation. This, together with the binding energy change of the Te 4*d* I core levels observed for $\Theta\leq2$ Å, argues for substrate-overlayer interdiffusion in this coverage range. The Hg depletion would be then related to the replacement of Hg—Te bonds with the more stable Cr—Te bonds. An independent check of this hypothesis can be obtained by comparing the observed attenuation of the Hg emission with the Cr atomic density. At $\Theta=2$ Å we have observed a 13—16 Å depletion layer at the film surface. The Te 4*d* II surface layer accounts for ~3 Å. The remaining 10—13 Å subsurface layer contains $\simeq(1.2-1.5)\times10^{15}$ Hg-sites/cm^2. At $\Theta\simeq2$ Å the Cr surface density is $\simeq1.67\times10^{15}$ atoms/cm^2. Therefore, the Hg attenuation is roughly consistent with a one-to-one exchange reaction between Cr and Hg atoms, followed by diffusion of the dissociated Hg away from the surface and subsurface layer.

The core binding energy results are more difficult to interpret due to the presence of a number of semiconducting and metallic species of rapidly varying composition. During the Hg-Cr exchange reaction the Te 4*d* I core shifts by about 0.25 eV to lower binding energy. This shift could reflect a net charge transfer to the Te atom because of the reduced Cr electronegativity compared to Hg. The *rigid* shift of the Te 4*d* I core level and the fact that the shift is independent of the experimental sampling depth (4 Å $<L<$ 8 Å for 110 eV $>h\nu>$ 53 eV) further confirms the picture of a Cr-Te reacted subsurface layer with a depth which is larger than L. The Cr 3*p* binding energy (Fig. 9) appears constant in the first interface formation stage ($\Theta\leq2$ Å), in agreement with a one-to-one exchange picture that yields a similar local environment for all Cr atoms in the subsurface region. After the reaction is completed, the Cr cores shift toward the bulk Cr position, as expected since no interdiffusion takes place for $\Theta\geq2$ Å. The Cr 3*p* binding energy for $\Theta\sim2$ Å is 0.5 ± 0.1 eV less than that for the final "metallic" position. This would seem to argue against a net charge transfer from Cr to Te atoms during the exchange reaction. We emphasize, however, that the observed "chemical shift" need not be related in an elementary way to the actual charge transfer.[24] Furthermore, for Cr atoms isolated in a nonmetallic matrix, as appears to be the case for $\Theta\leq2$ Å (Fig. 3), the binding energy should be measured from the vacuum level and would reflect the effective work function of the subsurface and surface species.[25] If we take, for example, the high coverage Cr 3*p* and Te 4*d* II binding energy as representative of the elemental Cr 3*p* and Te 4*d* emission, then at $\Theta\sim2$ Å both the Cr 3*p* core level and Te 4*d* I core levels exhibit an analogous ~0.5 eV shift to lower binding energy relative to the elemental state, with no clear indication of net charge transfer in any direction.

Exchange reactions between metal overlayers and semiconductor cations have been observed in II-VI compound semiconductors such as CdSe and CdTe.[1,2] In these materials dissociated Cd has been reported in the interface region and its presence has been related to the production of Ohmic contacts onto the semiconductor surface. These dissociated Cd species are characterized by a 0.5—0.6 eV *lower* 4*d* binding energy compared to Cd in the II-VI-semiconductor environment.[26] Our results show that the Cd emission from the $Hg_{1-x}Cd_xTe$-Cr interface decreases more slowly in intensity than the Hg emission, and that the binding energy of the Cd 4*d* cores seems to increase by about 0.3 eV at $\Theta=3$ Å. Therefore, while the subsurface region does contain a substantial amount of Cd, these atoms appear to be neither bulk-$Hg_{1-x}Cd_xTe$-like nor dissociated. A possible explanation is that the Cd atoms in the subsurface region interact with Cr when Cr replaces the neighboring Hg atoms with a charge transfer from Cd to Cr. Due to the higher stability of the Cd—Te bond as compared to the Hg—Te bond, the probability of Cr replacing Cd in the structure is smaller. If the exchange occurs, Cd atoms must migrate away from the subsurface region since we have no evidence of dissociated Cd within the experimental sampling depth. Both Cd and Hg, in fact, exhibit large diffusion coefficients in $Hg_{1-x}Cd_xTe$ at room temperature.[6] From the reduction in intensity of the Cd emission at $\Theta\sim2$ Å we can estimate a lower limit for this Cr-induced Cd deficiency in the subsurface layer of $(0.7-1.0)\times10^{14}$ atoms/cm^2. This would be consistent with the difference between the Cr surface concentration at $\Theta\sim2$ Å of 1.67×10^{15} atoms/cm^2 and the available Hg sites in the subsurface layer [$\sim(1.2-1.5)\times10^{15}$ atoms/cm^2]. In this picture, upon metal deposition Cr atoms would replace all of the Hg atoms and at least 20% of the Cd atoms in the subsurface layer. The model implies that the residual Hg 5*d* emission seen at $\Theta\simeq2$ Å is representative of the bulk semiconductor underlying the subsurface layer and its binding energy reflects the bulk stoichiometry and the near-surface band bending.[14] Systematic investigation with variable escape depth and high

resolution for the Cd 4*d* core levels is necessary to further verify the validity of this model.

CONCLUSIONS

The local morphology of the $Hg_{1-x}Cd_xTe(110)$-Cr interface is rather complex compared to those reported for the $Hg_{1-x}Cd_xTe$-Al and $Hg_{1-x}Cd_xTe$-Au interfaces. A description of this morphology was possible only through systematic studies of the core emission from each of the chemical species involved and, in particular, through careful line shape analysis of the Te 4*d* emission. Valence and core results are consistent with a first interface formation stage ($\Theta \lesssim 2$ Å) where Cr replaces all of the Hg atoms and at least 20% of the Cd atoms in a (10—13)-Å thick layer of the semiconductor. At the same time Te atoms are released from the semiconductor and form an elemental Te layer at the surface. When the exchange reaction is completed ($\Theta \sim 2$ Å), about $(1.2-1.5)\times 10^{15}$ Hg atoms in the subsurface layer have been replaced by Cr atoms. Further Cr deposition gives rise to a metallic Cr film covered by the dissociated Te species produced during the first stage of interface reaction (~ 1.3 monolayers). The typical high coverage interface morphology consists, therefore, of an elemental Te surface, a metallic Cr film, and a Hg-depleted 10—13 Å subsurface region where Cr—Te and Cd—Te bonds coexists, on top of the ternary semiconductor bulk. The Hg core emission from the underlying bulk remains at a constant binding energy indicating that the bulk environment and the semiconductor band bending[14] remain unchanged beneath the surface and subsurface layers.

ACKNOWLEDGMENTS

This work was supported, in part, by the Graduate School of the University of Minnesota under Grant No. 0100490832, by the Office of Naval Research, Department of the Navy, under Contract No. N00014-84-K-0545, and by the McDonnell Douglas Independent Research and Development program. We wish to acknowledge J. H. Hollister, B. J. Morris, and D. S. Wright for their assistance in sample preparation and characterization. We thank G. D. Davis and G. Margaritondo for useful discussions and for communicating their results to us prior to publication. Finally, we are grateful for the friendly support of the entire staff of the University of Wisconsin, Synchrotron Radiation Center at Stoughton (supported by National Science Foundation Grant No. DMR-76-15089).

[1]For an extensive review, see L. J. Brillson, Surf. Sci. Rep. **2**, 123 (1982).

[2]G. Margaritondo and A. Franciosi, Ann. Rev. Mater. Sci. **14**, 67 (1984) and references therein.

[3]W. A. Harrison, J. Vac. Sci. Technol. A **1**, 1672 (1983).

[4]A.-B. Chen, A. Sher, and W. E. Spicer, J. Vac. Sci. Technol. **A1**, 1675 (1983).

[5]W. E. Spicer, J. A. Silberman, I. Lindau, A.-B. Chen, A. Sher, and J. A. Wilson, J. Vac. Sci. Technol. A **1**, 1735 (1983).

[6]H. M. Nitz, O. Ganschow, V. Kaiser, L. Wiedmann, and A. Benninghoven, Surf. Sci. **104**, 365 (1981).

[7]A. Lastras-Martinez, V. Lee, J. Zehnder, and P. M. Raccah, J. Vac. Sci. Technol. **21**, 157 (1982).

[8]J. A. Silberman, D. Laser, I. Lindau, and W. E. Spicer, J. Vac. Sci. Technol. A **1**, 1706 (1983).

[9]G. D. Davis, N. E. Byer, R. R. Daniels, and G. Margaritondo, J. Vac. Sci. Technol. A **1**, 1706 (1983).

[10]R. R. Daniels, G. Margaritondo, G. D. Davis, and N. E. Byer, Appl. Phys. Lett. **42**, 50 (1983).

[11]J. A. Silberman, P. Morgen, I. Lindau, W. E. Spicer, and J. A. Wilson, J. Vac. Sci. Technol. **21**, 154 (1982).

[12]W. E. Spicer, J. A. Silberman, J. Morgen, I. Lindau, J. A. Wilson, An-Ban Chen, and A. Sher, Phys. Rev. Lett. **49**, 948 (1982).

[13]G. D. Davis, W. A. Beck, N. E. Byer, R. R. Daniels, and G. Margaritondo, J. Vac. Sci. Technol. A **2**, 546 (1984).

[14]D. J. Peterman and A. Franciosi, Appl. Phys. Lett. **45**, 1305 (1984).

[15]M. W. Scott, J. Appl. Phys. **40**, 4077 (1969).

[16]A.-B. Chen, A. Sher, and W. E. Spicer, J. Vac. Sci. Technol. **A1**, 1674 (1983).

[17]The reduced intensity of the Cd 4*d* emission at this coverage, the evident line broadening, and the emergence of a broad emission feature centered some 12.5 eV below E_F all yield some uncertainty in the estimate of the Cd 4*d* binding energy change. High-resolution photoemission studies of this coverage range are necessary before further discussion of this point.

[18]We will avoid using the expression "escape depth" to denote these parameters, since they do not represent the photoelectron escape depth at $h\nu = 60$ eV, as will become clear in the following discussion.

[19]These values for the escape depth of 4*d* photoelectrons from the Cr-Te overlayer are only rough estimates. See, for example, I. Lindau and W. E. Spicer, J. Electron. Spectrosc. **3**, 49 (1974).

[20]V. Solzbach and H. J. Richter, Surf. Sci **97**, 191 (1980).

[21]G. D. Davis, T. S. Sun, S. P. Buchner, and N. E. Byer, J. Vac. Sci. Technol. **19**, 472 (1981).

[22]M. Schlüter, J. D. Joannopoulos, M. L. Cohen, L. Ley, S. P. Kowalczyk, R. A. Pollak, and D. A. Shirley, Solid State Commun. **15**, 1007 (1974).

[23]Including the $\simeq 3$ Å Te 4*d* II layer.

[24]See, for example, R. E. Watson and M. L. Perlman, Struct. Bonding (Berlin) **24**, 82 (1975).

[25]P. H. Citrin and G. K. Wertheim, Phys. Rev. B **27**, 3176 (1983).

[26]C. F. Brucker and L. J. Brillson, Thin Solid Films **93**, 67 (1982).